



Experimental investigation of incipient shear failure in foliated rock



Matt J. Ikari ^{a, b, *}, André R. Niemeijer ^{c, d}, Chris Marone ^b

^a MARUM, Center for Marine Environmental Sciences, University of Bremen, Germany

^b Department of Geosciences, Pennsylvania State University, University Park, PA, USA

^c HPT Laboratory, Faculty of Geosciences, Utrecht University, Netherlands

^d Istituto Nazionale di Geofisica e Vulcanologia, Roma, Italy

ARTICLE INFO

Article history:

Received 20 January 2015

Received in revised form

27 April 2015

Accepted 11 May 2015

Available online 20 May 2015

Keywords:

Foliation

Rock fabric

Anisotropy

Fault

Friction

Shear strength

ABSTRACT

It has long been known that rock fabric plays a key role in dictating rock strength and rheology throughout Earth's crust; however the processes and conditions under which rock fabric impacts brittle failure and frictional strength are still under investigation. Here, we report on laboratory experiments designed to analyze the effect of foliation orientation on the mechanical behavior and associated microstructures of simulated fault rock sheared at constant normal stress of 50 MPa. Intact samples of Pennsylvania slate were sheared with a range of initial fabric orientations from 0 to 165° with respect to the imposed shear direction. Foliation orientations of 0–30° produce initial failure at the lowest shear stress; while samples oriented at higher angles are less favorable resulting in higher peak failure strength. In all samples, post-peak development of through-going deformation zones in the R1 Riedel orientation results in a residual strength that is lower than that observed for powdered gouge from the same material. As shear strain increases, all samples approach a residual apparent friction, defined by the ratio of shear strength to normal stress, of ~0.4. However, the final deformation microstructure depends strongly on the orientation of the pre-existing foliation. When fabric is oriented at low angles to the shear direction (<60°) slip occurs on the pre-existing foliation. Passive rotation of spectator regions becomes apparent for samples with foliation orientation of 60–90°. At higher foliation angles, deformation typically occurs in wide, through-going zones at an R1 orientation that cross-cuts the fabric or in a P-orientation along the fabric. These samples typically exhibit greater geometric layer thinning per unit shear strain. Our results document how pre-existing foliation, in any orientation, can lower the residual shear strength of rock. In contrast, the initial yield strength and peak failure strength of foliated rock is often higher in comparison with powdered samples of the same material, due to strength anisotropy and because activating slip on pre-existing foliation requires dilation and associated work against normal stress. The relationship between rock fabric orientation and frictional strength evolution that we document can explain how incipient faulting and/or flexural slip occur in foliated rock, especially when the orientations of fractures and original fabric vary widely.

© 2015 Elsevier Ltd. All rights reserved.

1. Introduction

Foliation and shear fabric are critical factors contributing to long-lasting mechanical weakness in fault zones. Internal fault zone structure is formed concomitant with deformation, and is thus an acquired, evolving characteristic. However, if the protolith has a pre-existing rock fabric, failure and slip in the early stages of faulting could be influenced by strength anisotropy. Such strength anisotropy

could be imparted by diagenesis, such as in shales, or due to previous deformation, such as in rocks like schists or mylonites. For example, inherited structure has been used to explain fault slip in situations where the fault is misoriented with respect to the current stress field, i.e. non-Andersonian faults. This includes dormant faults which are later reactivated in an opposite sense (i.e., reverse faults reactivated as thrusts and vice versa) (Sibson, 1985; Collettini and Sibson, 2001), and faulting in exhumed mylonites with unfavorably oriented foliation (Massironi et al., 2011; Bistacchi et al., 2012). Furthermore, field observations show that foliation orientation with respect to the maximum compressive stress strongly controls fault complexity and length-slip relationships (e.g. Butler et al., 2008).

* Corresponding author. MARUM, Center for Marine Environmental Sciences, University of Bremen, Germany.

E-mail address: mikari@marum.de (M.J. Ikari).

Slip on pre-existing foliation is common during folding. A simple example is bedding-parallel slip that occurs in fold limbs (Ramsay, 1974; Bell, 1986; Tanner, 1989; Becker, 1994; Davis and Forde, 1994; Fagereng and Byrnes, 2015). Such slip can sometimes be induced during earthquakes (Klinger and Rockwell, 1987; Berberian et al., 1994; Lee et al., 2002). In some cases, seismicity can preferentially nucleate on pre-existing foliation, as seen in earthquake swarms within the mylonitic belts of northeastern Brazil (Ferreira et al., 2008).

Previous studies have measured the compressional strength of foliated or fractured rocks in triaxial configurations, showing that strength is lowest when the fabric is oriented $\sim 30^\circ$ to σ_1 , the axis of greatest compressive stress. This corresponds to the point at which fabric is aligned with typical angles for Coulomb failure (e.g. Donath, 1961; Hoek, 1964; Handin, 1969; Attewell and Sandford, 1974). However, for natural faults where shear is distributed within a zone of finite thickness, the stress state can vary strongly and non-coaxially across the shear zone; in particular where internal fabric develops within shear zones (e.g., Mandl et al., 1977; Hobbs et al., 1990; Byerlee and Savage, 1992; Scott et al., 1994; Marone, 1995; Ikari et al., 2011; Rathbun and Marone, 2010; Haines et al., 2013). For active shear failure within a fault zone of finite, constant width the principal stress axes are oriented 45° relative to the remotely applied stresses rather than coaxial and can vary if the fault zone width changes. Microstructural observations of experimentally sheared fault material show that in addition to fault-parallel shear planes or boundary shears, other deformation features can develop at nearly any orientation (Logan et al., 1992; Haines et al., 2013). In natural fault zones, examples include R1 (Riedel) shears, P-foliation and other structures (Rutter et al., 1986; Cladouhos, 1999; Logan, 2007).

Experimental friction studies in which foliated rock or gouge is sheared have focused primarily on foliation that is aligned parallel to the shear direction. These studies have shown that fault-parallel fabric can significantly reduce strength, even when the proportion of intrinsically weak minerals is limited (Niemeijer and Spiers, 2005, 2006; Collettini et al., 2009; Niemeijer et al., 2010; Ikari et al., 2011). Intense planar fabric is sometimes observed in the cores of highly localized, phyllosilicate-rich faults and thus may be an effective weakening mechanism in natural faults (Chester et al., 1985; Collettini and Holdsworth, 2004; Jefferies et al., 2006; Frost et al., 2011). However, it is unclear if such extreme localization is specific to mature fault zones, given that in many cases gouge zone thickness appears to scale with net offset even for faults with large displacements (Scholz, 1987; Hull, 1988). Moreover, it is unclear how fault strength is affected by pre-existing fabric at low strains, when syn-deformational microstructure is more complicated. Thus, if fabric development is tied to strain weakening a key unresolved question concerns whether weakening leads to fabric development or vice versa.

Here, we measure the frictional strength of a foliated rock, specifically Pennsylvania black slate, at low shear strain ($\gamma < 4$) and consider original fabric orientations of 0 – 165° with respect to the shear direction. We integrate our mechanical results with observations of microstructural deformation in order to explore the effect of pre-existing rock foliation on fault strength, strain weakening, and microstructural evolution.

2. Methods

2.1. Experimental procedure

We conducted experiments in a biaxial shearing apparatus to measure the evolution of shear strength with displacement under controlled normal stress and sliding velocity (e.g. Ikari et al., 2011).

Two intact, prismatic layers of Pennsylvania black slate were sheared within a three-piece steel block assembly in a double-direct shear configuration. Data reported here represent values averaged for the two individual sample pieces (Fig. 1). The forcing block surfaces were grooved (0.8 mm deep and with a 1 mm wavelength) to ensure that shearing occurred within the layer and not at the layer–block interface. In all experiments, the normal stress σ_n was maintained at 50 MPa and the contact area was maintained at 25 cm^2 at room humidity ($\sim 40\%$) and temperature ($\sim 25^\circ \text{C}$). Our slate samples are shown by X-Ray Diffraction (XRD) to be composed of 54% phyllosilicate minerals (40% illite, 14% chlorite), 31% quartz + feldspar (albite) and 15% calcite + dolomite. Foliation intensity was measured using X-Ray Texture Goniometry (XTG) as having a Multiples of Random Distribution (MRD) of 7.8–7.9, which is typical of slates (Haines et al., 2009). Solid wafers with the dimensions $5 \times 5 \times 1 \text{ cm}$ were cut from intact rock specimens with pre-existing foliation at angles of 0 – 90° to the long axis in 15° increments. We sheared samples at a range of orientations, with foliation oriented from 0 to 165° to the applied shear stress (Fig. 1, Table 1).

In each experiment, the sample was sheared initially at a constant velocity of $11 \text{ }\mu\text{m/s}$ and to total displacements of 21.5 – 26.5 mm (as recorded at the gouge boundary) which resulted in bulk engineering shear strains of $\gamma = 2.9$ – 3.5 (disregarding shear localization). Shear strain is calculated as $\gamma = \Sigma(\Delta x/h)$, where x is the shear displacement and h is the instantaneous layer thickness. Instantaneous layer thickness is calculated from the layer thickness measured after application of normal load but before shearing (~ 9 – 10 mm , Table 1), and the normal displacement throughout the experiment. Residual steady-state shear stress τ was generally attained at shear strains of ~ 1.5 – 2.5 , although the samples exhibited significant variation in residual friction. After reaching steady-state friction, velocity-stepping tests were initiated, in which shearing velocity was instantaneously stepped from 1 to 3 , 10 , 30 , 100 , and $300 \text{ }\mu\text{m/s}$. Shear displacement during each velocity step was $500 \text{ }\mu\text{m}$.

2.2. Friction measurements

We report values of the apparent coefficient of sliding friction μ_a , calculated as:

$$\mu_a = \tau / \sigma_n \quad (1)$$

The measured shear stress τ includes the contributions of both the true internal coefficient of friction and cohesive strength, however since we cannot quantify the proportion of each quantity we report and compare values of apparent friction (Byerlee, 1978). We report the apparent coefficient of friction because the thickness of experimental fault zones is known to influence measured frictional strength (Scott et al., 1994; Marone, 1995; Ikari et al., 2011), therefore we expect that our apparent friction values may be lower than the true values. However, because we use only one sample type and sample thicknesses were uniform (9.0 – 10.5 mm under application of normal load) we can compare measured friction values across our sample suite. Rates of layer thinning, normalized by layer thickness, were calculated continuously as $W = -\Delta h/h\Delta x$ (mm^{-1}). Increasingly positive values of W indicate compaction (thinning), while decreasing W indicates dilation. In the biaxial testing configuration we use here, thinning occurs throughout the experiment, much of which is due to extrusion as material is left behind in the trailing portion of the layer (e.g. Scott et al., 1994). However because we employ a consistent initial sample thickness, we may compare values of W across our experimental suite.

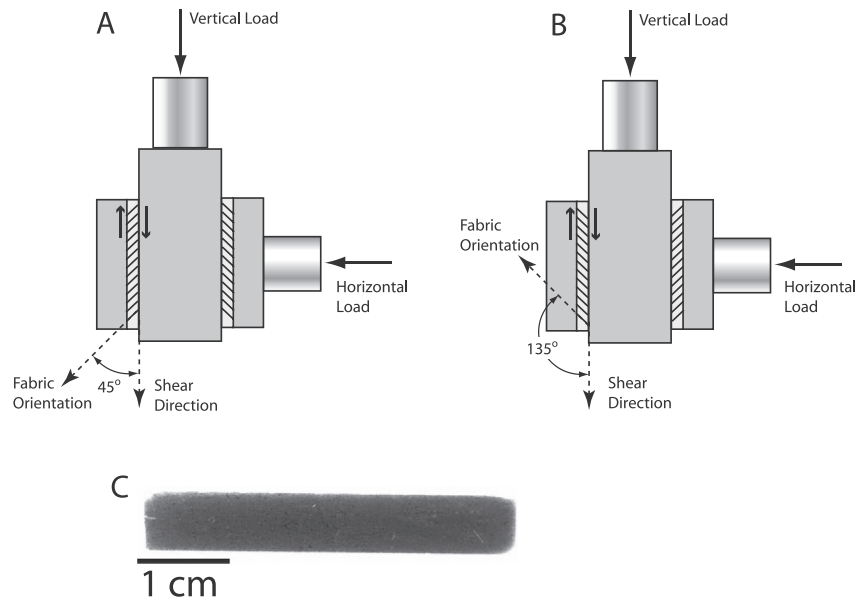


Fig. 1. Double-direct shear geometry and definition of rock fabric orientation relative to shear: (A) foliation at 45° to the shear direction, (B) 135° to the shear direction. (C) Pennsylvania slate prior to deformation, representing the starting material. Initial foliation (horizontal) is not easily discernible due to lack of fractures and low porosity.

In the post-peak portion of the test after attainment of residual sliding friction, we quantify the response of friction to step-wise increases in load point velocity from V_0 to V using the parameter $a-b$, where:

$$a - b = \frac{\Delta\mu_a}{\ln(V/V_0)} \quad (2)$$

which is a reduced form of the rate-state friction (RSF) law (Dieterich, 1979, 1981; Ruina, 1983) for steady-state conditions. A material exhibiting a positive value of $a-b$ is said to be velocity-strengthening, and will tend to slide stably, while a material with negative $a-b$ is termed velocity-weakening, which is considered to be a prerequisite for frictional instability that may result in earthquake nucleation (e.g., Scholz, 2002).

Following the friction tests, samples were removed from the forcing blocks of the double direct shear configuration and impregnated with epoxy (Buehler EpoThin® resin and hardener). The epoxied samples were cut parallel to the shear direction,

polished, and imaged with a high resolution scanner. In most cases, impregnation of the sample was incomplete, likely due to reduced permeability from the production of fine-grained comminuted material.

3. Results

3.1. Rock friction

The friction-displacement behavior for the slate samples is typical of fault materials, with a period of quasi-elastic loading followed by yielding, a peak stress and strain weakening (e.g., Marone, 1998). Our suite of samples exhibits a systematic range of behaviors as a function of the variation in foliation angle with respect to the shear direction (Fig. 2). A common characteristic of intact slate samples is that regardless of orientation, sample failure is signaled by an early peak and subsequent drop in strength, after which a residual level is reached (Fig. 2). This behavior differs from that of powdered slate tested using the same experimental

Table 1
Experimental details and results.

Experiment	Angle to foliation (°)	Initial thickness (mm)	Thickness under load (mm)	Failure (peak) μ_a	Residual μ_a	Failure W ($\gamma < 0.5$) (mm^{-1})	Residual W ($\gamma > 1$) (mm^{-1})	$a-b$ ($\times 10^{-3}$)
p2673s14sl50	powder	13.83	6.11	0.41	0.41–0.49	0.024–0.040	0.023–0.024	1.5–2.8
p3164s10sl50	0	10.14	9.87	0.39	0.35–0.37	0.015–0.025	0.018–0.024	1.0–3.8
p2551s10sl50	15	10.03	9.72	0.43	0.40	0.019–0.029	0.023–0.025	0.6–1.7
p2544s10sl50 ^a	15	9.96	9.39	0.40	0.38–0.39	0.021–0.029	0.026	1.2–2.3
p2541s11sl50	30	10.76	10.46	0.47	0.44	0.022–0.032	0.022–0.026	0.5–2.1
p2538s10sl50	45	10.08	9.73	0.53	0.45–0.48	0.010–0.028	0.027–0.028	0.2–1.9
P2543s10sl50	60	10.29	10.00	0.53	0.30–0.38	–0.003–0.028	0.024–0.030	1.1–2.0
p2547s10sl50	75	10.36	9.99	0.34	0.33–0.37	–0.008–0.008	0.035–0.040	1.0–2.0
p2549s10sl50 ^a	75	10.03	9.72	0.39	0.37–0.39	–0.002–0.005	0.034–0.035	0.2–1.6
p2562s09sl50	90	9.38	9.21	0.40	0.37–0.38	0.002–0.007	0.031–0.038	1.1–2.0
p2546s10sl50	105	9.94	–	0.42	0.35–0.39	0.018–0.021	0.036–0.038	1.2–2.8
p2542s10sl50	120	10.03	9.54	0.56	0.38–0.39	0.014–0.025	0.034–0.036	1.0–3.0
p2539s09sl50	135	9.47	9.16	0.51	0.37–0.39	0.010–0.018	0.030–0.035	1.4–3.0
p2540s09sl50	150	9.22	9.02	0.53	0.38–0.39	0.003–0.024	0.033–0.034	0.3–2.3
p2545s10sl50	165	10.09	9.48	0.49	0.39–0.40	0.009–0.019	0.023–0.026	0.9–2.4

^a Repeated experiments included to demonstrate reproducibility.

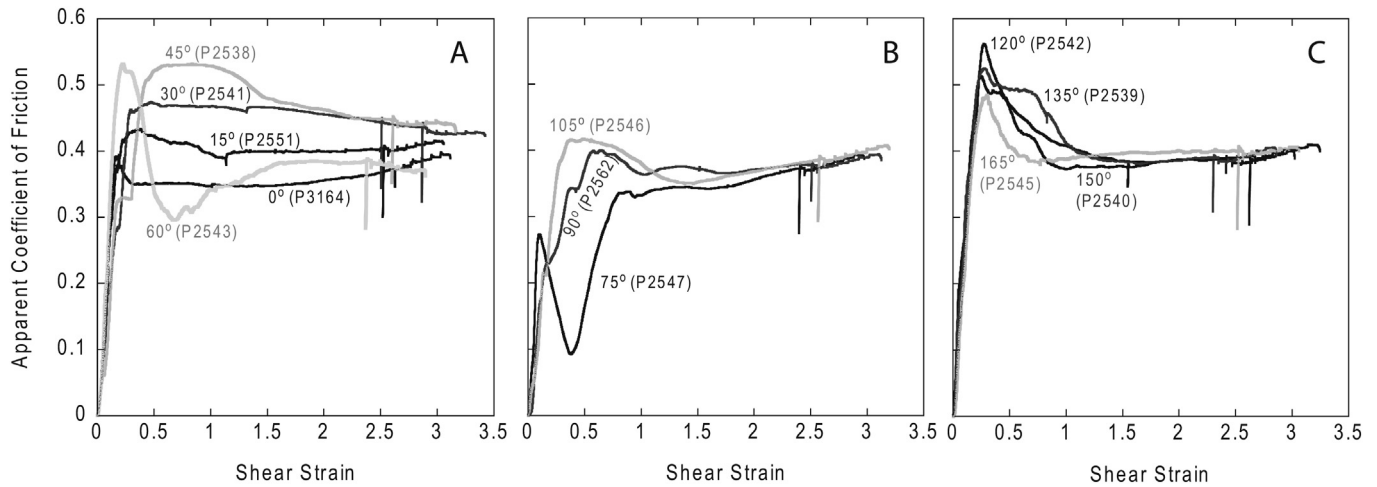


Fig. 2. Apparent friction coefficient μ_a as a function of shear displacement for fabric oriented at angles of: (A) 0–60°, (B) 75–105°, and (C) 120–165° to the shear direction. Apparent friction is calculated as shear stress divided by normal stress (50 MPa in all cases).

methods, which tends to lack a clear peak and exhibits continuous strain hardening (Colletini et al., 2009; Ikari et al., 2011).

We observe that the frictional strength of our slate samples varies significantly at low strain ($\gamma \leq 1$), but these differences fade at higher strain and residual friction approaches a constant value (Fig. 2). For low angle fabric orientations (0–45°), frictional strength is highly variable over the course of a single experiment, and the pre-existing fabric has a strong and long lasting effect on friction (Fig. 2). As the orientation of the pre-existing fabric increases, the friction–strain profiles become more similar at progressively lower strain. For fabric orientations of 75–90° and higher, the friction curves are variable but after shear strains of ~ 1 the curves converge to become nearly identical (Fig. 2B). The sample with fabric at 75° exhibits unusual strength–strain behavior (Fig. 2B). In this instance failure strength is very low, followed by a pronounced strength drop and then an evolution to a residual apparent friction value that is higher than the peak stress. Repeated experiments verify that this apparently anomalous behavior is reproducible (Table 1). At $\geq 120^\circ$, the evolution of friction is similar for all samples throughout the experiment (Fig. 2C).

The apparent coefficient of friction at failure (peak friction) ranges between 0.34 and 0.56 (Fig. 3, Table 1). As a function of fabric

orientation with respect to shear direction, failure μ_a increases from 0° to 60°, abruptly drops to a minimum value at 75° and then increases again at higher angles (Fig. 3). In cases where the residual apparent friction is not clear, we report two values as upper and lower bounds (Fig. 3B). These values generally range between 0.3 and 0.5, but the upper bound in residual μ_a is approximately constant at ~ 0.38 for 60°–180° (or 0°). Lower bounds in residual μ_a for these orientations are also fairly constant, generally within 0.02 of the upper bound, with the exception of orientations of 60° and 75° (Fig. 3B). From 0° to 45°, residual friction increases systematically, with μ_a reaching 0.48. When compared to friction values of powdered slate with similar initial thickness (Ikari et al., 2011), failure μ_a values for intact samples are generally higher (failure μ_a of powdered slate = 0.41) while all the residual μ_a values are lower (residual μ_a of powdered slate = 0.49).

We find that shear strength correlates strongly with changes in layer thickness. In a typical experiment, the layer compacts and thins as the shear stress increases upon initial loading (Fig. 4A). The thinning rate W increases to a “peak” value before the peak strength and subsequently decreases to a minimum value that coincides with the peak strength, signaling dilation of the sample (e.g., Marone, 1991) and corresponding with the onset of yielding

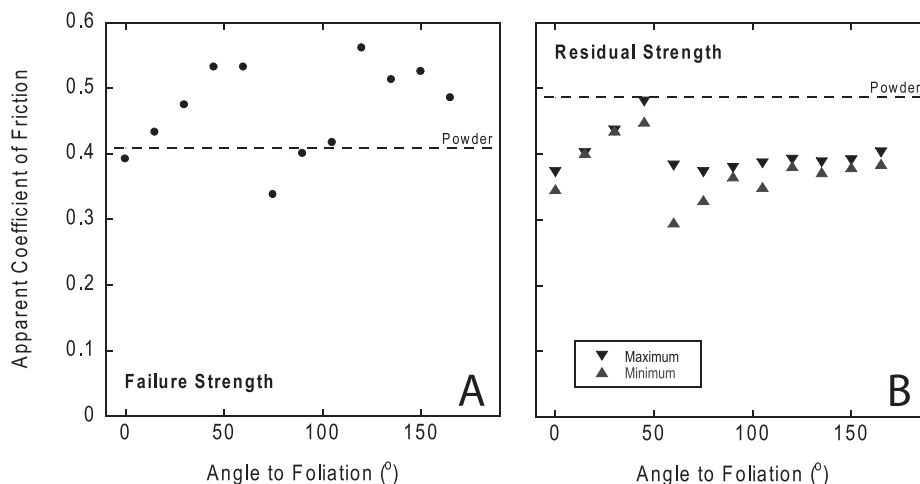


Fig. 3. (A) Apparent friction μ_a at failure, and (B) Residual apparent friction. Dashed lines indicate apparent friction values for powdered slate (Ikari et al., 2011) as a reference.

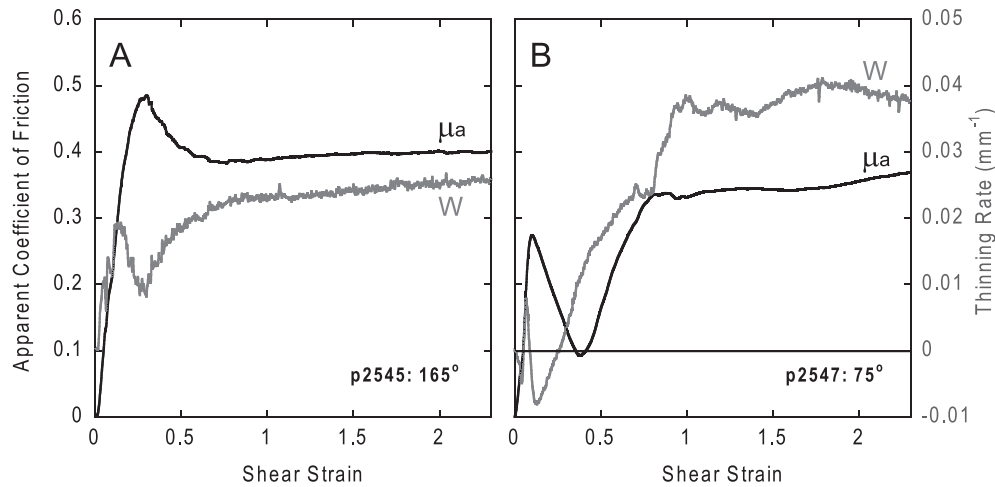


Fig. 4. Comparison of apparent friction μ_a and thinning rate W as a function of shear strain for samples sheared (A) 165° to original foliation, representing a typical experiment; and (B) 75° to original foliation.

(Fig. 4A). After failure, thinning resumes and eventually reaches a residual level at shear strains that coincide with the attainment of residual friction levels ($\gamma > 1$), consistent with concepts from critical state soil mechanics and expectations based on the total work of deformation (e.g., Scholz, 2002; Craig, 2004). This direct correlation between strength and thinning rate also holds for the sample with a foliation orientation of 75°, which exhibits anomalous frictional behavior (Fig. 4B). Values of the maximum or “peak” thinning rate are typically measured at $\gamma \leq 0.2$, and minimum values at $\gamma \leq 0.5$. These low-strain W values increase from 0.015 to 0.025 mm^{-1} for foliation orientations of 0°–30°, then sharply decrease (Fig. 5A, Table 1). The negative W at 60° and 75° signifies large overall dilation, with maximum W of 0.025 and minimum values as low as 0.003 mm^{-1} . For the residual values of W , measured once the samples have reached residual friction levels, we report upper and lower bounds (Fig. 5B, Table 1). From fabric orientations of 0°–60°, W increases from ~0.023 to ~0.030 mm^{-1} . A maximum thinning rate of ~0.040 mm^{-1} occurs at 75°, after which W decreases back to ~0.023 mm^{-1} as the angle between foliation and shear direction increases. Values of W for samples oriented between 75° and 150° are clearly higher than those at orientations of 45° and below. This

pattern is significantly different than that observed in the friction data, which show higher strength at lower angles. For all tested slip velocities, the friction rate parameter $a-b$ is positive and ranges from ~0 to 0.004 (Fig. 6, Table 1). There is no significant dependence of $a-b$ on fabric orientation, but the values are generally slightly lower than the range for powder based on Ikari et al. (2011).

3.2. Microstructural analysis

We adopt the nomenclature of Logan et al. (1992) to describe the microstructure of our sheared samples (Fig. 7). For samples with foliation approximately parallel to the shear direction (0°), fractures are generally in the R1 orientation but range from ~30° near the trailing edge of the sample (where shear strain is lower, due to larger thickness and lower displacement prior to being left behind), to nearly sub-parallel to shear (and foliation) near the central part of the sample (Fig. 8), consistent with previous works that have documented the strain distribution in laboratory shear zones (Rathbun and Marone, 2010). Deformation appears to be asymmetric across the sample width, being more highly strained at the top of the micrograph (Fig. 8), which corresponds to the surface in contact with the side forcing block of the double direct shear

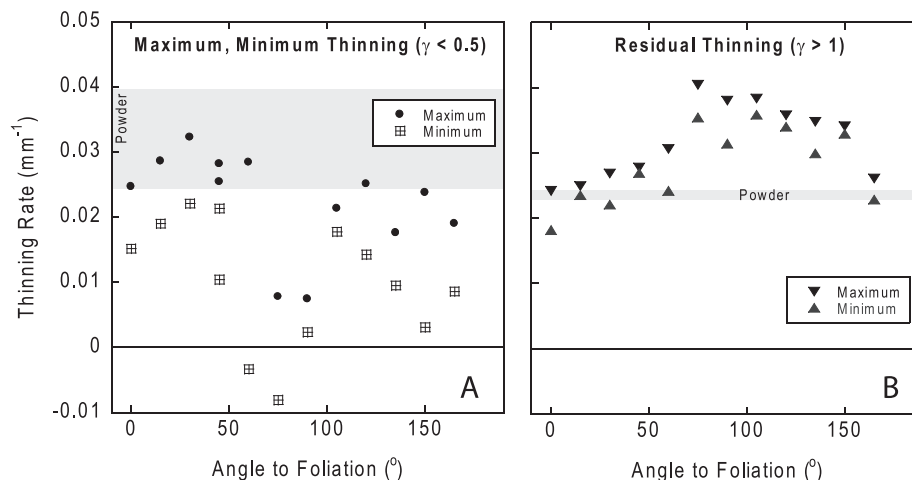


Fig. 5. Normalized thinning rate W as a function of fabric orientation at (A) low shear strains of $\gamma < 0.5$ corresponding with peak friction, and (B) higher shear strains of $\gamma > 1$ corresponding with residual friction. Gray bands indicate range of W values for powdered slate (Ikari et al., 2011) as a reference.

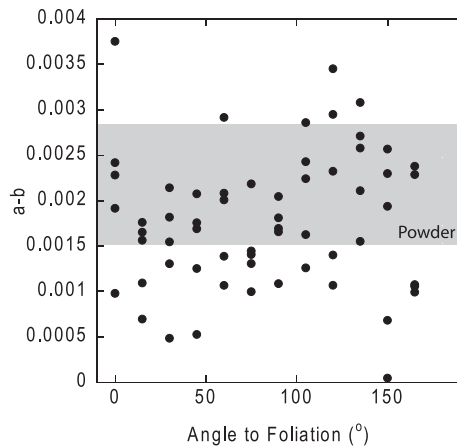


Fig. 6. Rate-dependent friction parameter $a-b$ as a function of fabric orientation angle. For each orientation, the five data points represent the range of tested slip velocities. Gray band indicates range of $a-b$ for powdered slate (Ikari et al., 2011).

assembly (Fig. 1). This is also evident from observed streaks of light colored material, likely calcite or dolomite.

When the original foliation is oriented 15–45° from the shear direction, foliation-parallel fractures are apparent throughout the samples (Fig. 8), which we interpret to be indicative of foliation-parallel slip. As foliation orientation increases, fracturing along foliation planes becomes more common. Generally, this occurs in the trailing portion of the sample (e.g. left side of the 30° and 45° sample micrographs, Fig. 8) and sometimes in the leading portion (e.g. right side of the 45° and 60° sample micrographs, Fig. 8). In the central part of the samples, little fracturing is observed and porosity appears to be lower. This apparently compactive deformation occurs in wide zones that tend to be roughly in the R1 orientation and appear to become listric, curving toward the sample boundary (Fig. 8).

As the foliation orientation increases to 60–90°, these wide, R1-oriented zones of deformation become larger, and tend to have sharper, more planar boundaries oriented at 30° (Figs. 8 and 9). A striking feature in these samples is the rotation of passive, less-deformed “spectator” regions outside the wide central deformed zones, which is most clear in the trailing edge “footwall” areas. For example, compare the lower left footwall area of the 60° sample in which the fabric has rotated to ~105–120° with the upper right hanging wall area, which retains the original fabric orientation (Figs. 8 and 9). Within the highly deformed zones, the rock appears to be highly comminuted and some samples exhibit wavy, flow-like structures. Overall fabric appears to have obtained a P-foliation (60°) or X-foliation (75°, 90°). Boundary shears are prominent within this zone for these samples.

Samples with foliation oriented $\geq 105^\circ$ display similar characteristics to those with foliations of 60–90°, however little to no rotation of the outer spectator regions occurs (Fig. 9). Open fractures are relatively uncommon and are restricted to outer portions of spectator regions. Central deformed zones appear to become more listric and attain lower angles toward the leading edge of the sample (where strain is higher). Within these zones, foliation is often anastomosing and has a P orientation. These samples are generally similar and develop consistent microstructures. For powdered slate, little deformation fabric is observed other than very faint through-going R1 shears, which are nearly invisible compared to the initially intact rock samples (Fig. 10).

4. Discussion

4.1. Relation between fabric orientation, rock friction, and microstructural development

4.1.1. Low-strain deformation: comparison with compressional experiments

A consistent result from existing triaxial compression studies on foliated rock is that compressive strength decreases as foliation angle decreases from 0° to the maximum compressive stress σ_1 to a minimum at a foliation angle of ~30° to σ_1 , then increases as the angle of foliation approaches 90° (cf. Fig. 4) (e.g. Donath, 1961; Hoek, 1964; Attwell and Sandford, 1974). In our samples, the principal stress axes rotate as shear stress increases from 0 to failure such that σ_1 and σ_3 (minimum compressive stress) are oriented ~45° from the remotely applied stresses during shear failure (Mandl et al., 1977; Hobbs et al., 1990; Byerlee and Savage, 1992; Scott et al., 1994; Marone, 1995; Ikari et al., 2011). Therefore, Coulomb failure planes oriented $\pm 30^\circ$ from σ_1 correspond with 15° (R1 orientation) and 75° to the shear direction (R2).

We observe increasing failure strength as the original rock foliation orientation increases from 0 to 45° with respect to the shear direction (Fig. 4). At shear failure (or maximum shear stress), the principle stress axes have completed their rotation. From triaxial experiments using isotropic rock cylinders with a sawcut of varying orientation, Handin (1969) found that sliding was favored over development of new fractures when the sawcut was oriented 30–60° from σ_1 . In our apparatus, this corresponds to foliation orientations of 0, 15, and 165°. Handin (1969) did not test sawcut angles $< 30^\circ$ from σ_1 , however we expect that our sample with fabric oriented at 30° (15° from σ_1) may behave similarly. Therefore, we suggest that the low failure friction we observe for foliation orientations of 0–30° and 165° ($\mu_a < 0.5$) is the result of fabric-parallel slip since the fabric is favorably oriented with angles typical of Coulomb failure (Fig. 11). This is in good agreement with previous strength measurements on foliated rock in the triaxial configuration, which show a characteristic minimum strength at ~30° (e.g. Donath, 1961; Hoek, 1964; Attwell and Sandford, 1974).

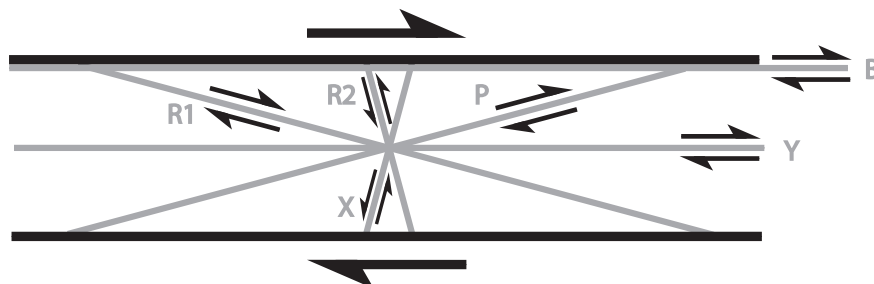


Fig. 7. Schematic representation of deformation microstructure showing the orientation of potential localization features and their nomenclature following Logan et al. (1992).

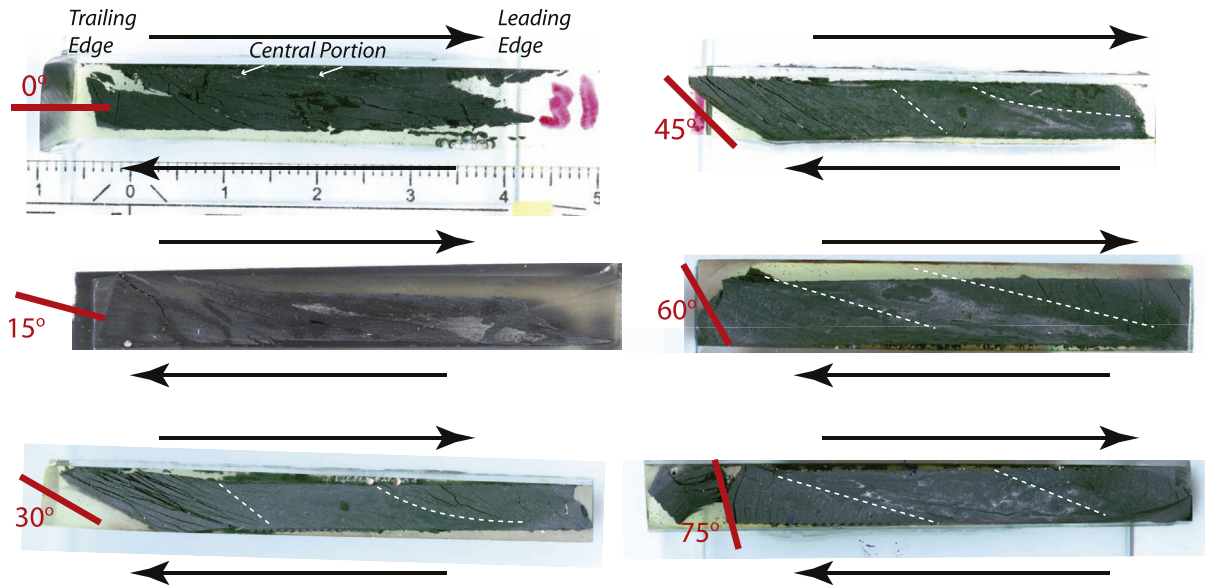


Fig. 8. Scanned images of deformed samples with foliation oriented from 0° to 75°. Scale in cm. White arrows on 0° sample show streaks of light-colored material (calcite or dolomite, see text). Dashed lines delineate the low-porosity “compactive zone” for the 45° sample.

The increase in failure friction from 0 to 60° is likely caused by increasing misalignment of fabric with optimal Coulomb failure angles. From 75 to 105°, failure friction is considerably lower than at all other fabric orientations. These foliation orientations are also 30–60° from σ_1 , therefore the low failure strength in these samples may also be the result of foliation parallel slip. In this case, foliation parallel slip at low strain occurs in the antithetic R2 orientation. Additionally, because our samples have a fairly large initial thickness, the layers experience a rotational moment and thus both spectator regions and foliations rotate with shear, as observed in the microstructures (Figs. 8, 9 and 11). At foliation orientations of 120–150°, failure strength is likely high because of severe misalignment of σ_1 with respect to Coulomb failure angles causes fractures to develop that cross-cut the original fabric early in the strain history (Figs. 9 and 11).

We observe what appears to be anomalous frictional behavior for fabric at 75° to the shear direction, and to a lesser extent for

samples with fabric 60° to the shear direction. This unusual stress-strain behavior includes a large drop in friction following an initial peak (Fig. 2). However, the thinning rate still correlates with apparent friction (Fig. 3B). These particular samples exhibit low minimum friction values, as well as values of thinning so low they exhibit net dilation (Figs. 4 and 5). This is confirmed by the microstructural observations, which show clear evidence of rotation from being inclined to the shear direction (60–75°) to against the shear direction (105–120°) (Fig. 8). Therefore, we suggest that the premature drop in friction and associated dilatancy is a consequence of this particular fabric orientation where rotation is more favorable than shear.

4.1.2. Deformation at higher strain

At higher strains, after residual friction values are reached, the mechanical behavior is very different from that observed for lower strains (Fig. 2). Residual friction increases from 0.37 to 0.48 as the

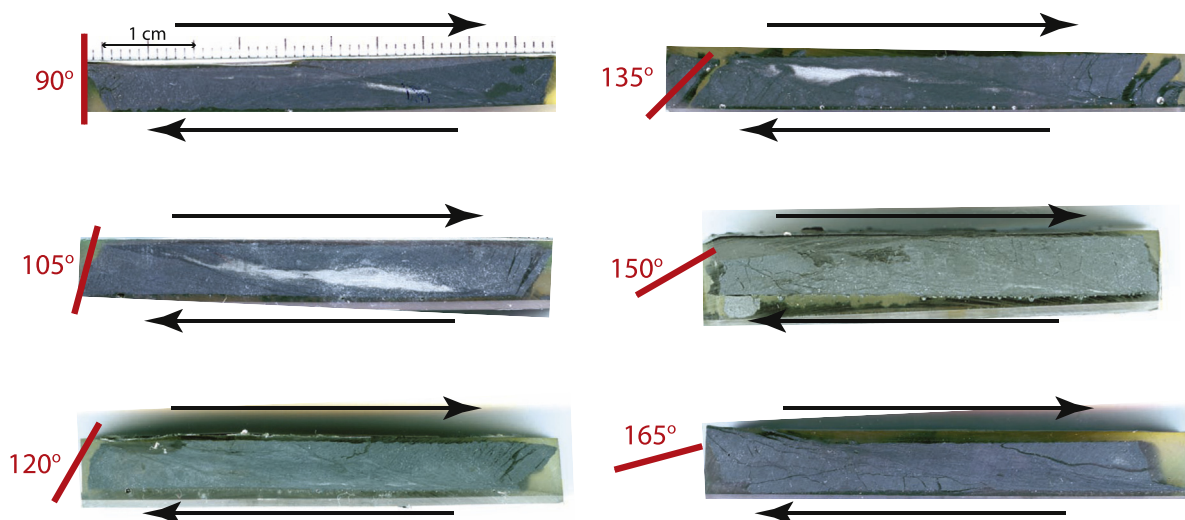


Fig. 9. Scanned images of deformed samples with foliation oriented from 90° to 165°. Scale in cm.

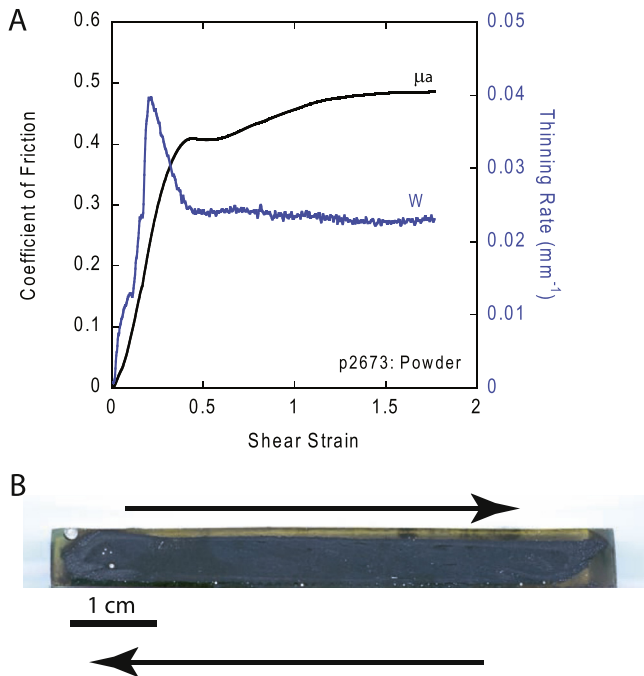


Fig. 10. (A) Apparent coefficient of friction μ_a and thinning rate W as a function of displacement for a slate sample tested as powdered gouge (Ikari et al., 2011), and (B) Scanned image of the deformed powdered gouge.

foliation orientation increases from 0 to 45°, then abruptly decreases to ≤ 0.40 at all other orientations. We suggest that the low residual friction at higher foliation orientations is the result of deformation accommodated in wide, through-going shear zones in the R1 orientation, probably assisted by slip on fabric in the P-orientation (Figs. 9 and 11). This is consistent with the fact that an original fabric oriented $\geq 120^\circ$ from the shear direction is unfavorably oriented for reactivation (e.g., Sibson, 1985; Collettini and Sibson, 2001), and therefore through-going deformation in the R1 orientation is forced to form early. Due to kinematic constraints in the direct shear configuration, foliation-parallel slip in the R2 orientation is inhibited compared to R1, so through-going deformation also occurs earlier for samples with foliation oriented at 75–105°. We suggest that the higher residual friction for samples with fabric oriented 15–45° is the result of a rotational moment experienced by the sample, which induces foliation perpendicular compression. This is supported by the microstructures, which indicate that samples with foliations oriented at 15–45° develop central zones that lack open fractures and thus have lower porosity. Eventually, we expect continuous deformation that cross-cuts the rock fabric to form at higher strain (Fig. 11).

Measurements of thinning rate during shear provide further evidence that the strength and structure of faults is controlled by the fabric of the actively shearing zone. At low strains (during initial failure), thinning rates are slightly larger at orientations $\leq 60^\circ$ compared to $\geq 75^\circ$, which we suggest is the result of sliding on favorably oriented fabric at low orientations. This pattern of dependence of the thinning rate W is reversed at high strains where friction reaches residual values (Fig. 5). For foliation orientations $\leq 60^\circ$, values of W are significantly lower than when the foliation is oriented $\geq 75^\circ$. This is easily explained considering that samples with lesser early thinning likely experience more thinning later. Additionally, the trend of increasing thinning rates from 0 to 45° may be attributed to compaction and porosity reduction. However, at very high foliation orientations, the pre-existing fabric becomes

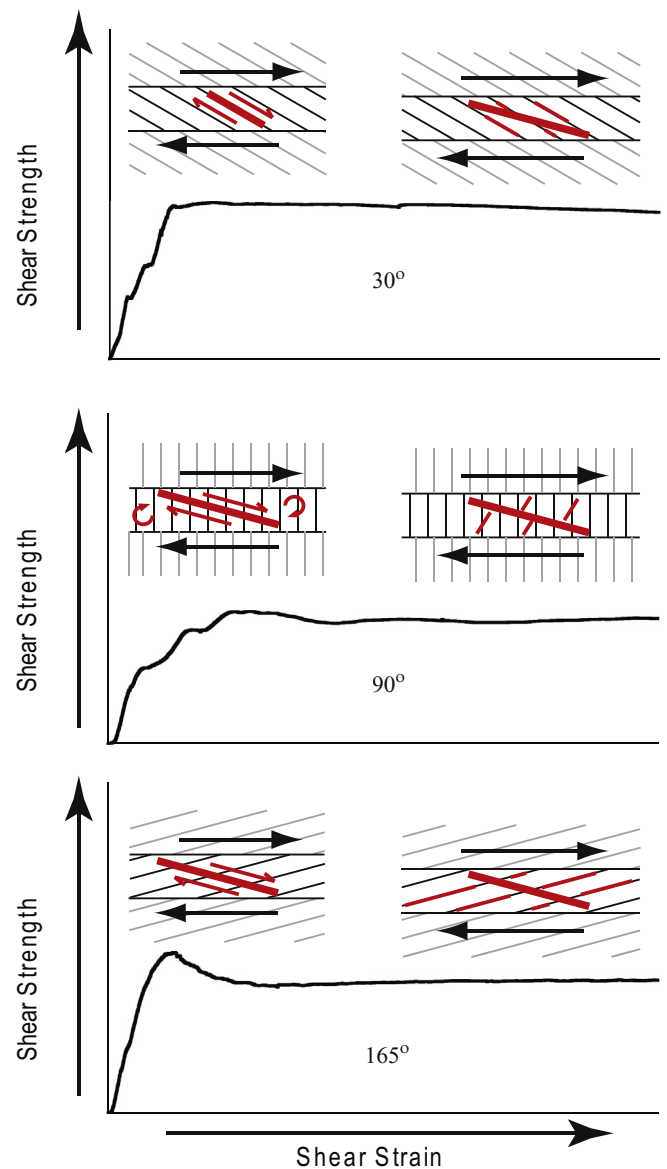


Fig. 11. Schematic illustration showing deformation patterns (in red) with respect to original rock foliation, and corresponding evolution in frictional strength with increasing shear strain for samples with foliation oriented at 30, 90, and 165°. (For interpretation of the references to colour in this figure legend, the reader is referred to the web version of this article.)

consistent with P-foliation. Slip on foliation in the P-orientation would offset some thinning on R1-shears (Cladouhos, 1999), which may explain the decline in thinning rate as foliation orientation increases from 75 to 165°.

4.2. Foliated rock deformation in nature

Our results indicate that protolith and initial fault zone fabric play a significant role in determining frictional behavior and microstructural development of foliated fault rocks. These effects are expected to be greatest for low strain and immature faults forming in a foliated protolith. Our study extends several recent works that used a similar experimental configuration to investigate intact, foliated rocks and specifically the effect of foliation parallel to the shear direction (0°) (Collettini et al., 2009; Carpenter et al., 2011; Ikari et al., 2011; Tesei et al., 2012). The effect of rock

foliation on friction is particularly evident when comparing the samples in this study with initially structureless, powdered slate (Fig. 3B). Due to the strain-hardening nature of the powder as opposed to peak-decay behavior for intact slate samples, the powder, in general, has a lower failure strength and higher residual strength. Therefore, using results from powdered gouge to estimate the strength of natural foliated rocks in a fault zone could lead to over- or under-estimation depending on the amount of accumulated shear strain.

One example where pre-existing foliation is important during the deformation process is flexural slip during folding (Ramsay, 1974; Tanner, 1989). In this case, the shortening is partially accommodated by bedding-parallel slip in the fold limbs. However, rotation and shear of individual “beams” within the limbs means that deformation is often accommodated on foliations that are not coaxial with the dip of the limbs (e.g. Bell, 1986). Furthermore, recent studies have shown that flexural slip can occur on steeply dipping, unfavorably oriented foliation planes (Fagereng and Byrnes, 2015). While a detailed assessment of foliation effects on various crenulation arrangements is beyond the scope of this work, we suggest that our results are consistent with the idea that during flexural slip, displacement occurs along both bedding planes and relict fabrics whose orientation may vary widely compared to original bedding. Our results show that foliation at any orientation lowers residual rock strength. Therefore we suggest that this weakness may contribute to the reactivation of crenulation fabrics, often over multiple episodes of deformation, which is observed in field analyses (Bell, 1986; Davis and Forde, 1994; Ham and Bell, 2004).

We show that in wide shear zones with an inherited microstructure, shear deformation is accommodated by both incipient shear planes and pre-existing fabric. In mature faults with large offset, the original foliation would eventually be destroyed by comminution, textural overprinting, and authigenic mineral growth. It is unclear how much strain is necessary to fully eradicate the influence of pre-existing fabric, however this is likely to occur when slip becomes fully concentrated on boundary or Y-shears, when deformation in the rest of the fault zone is not necessary to accommodate further offset. Dynamic rupture is also expected to be a factor in resetting fabric evolution in shear zones. Brecciation, fracture branching and dynamic, process-zone strain gradients are likely to erase or significantly modify fault zone fabric (Sibson, 1986). Our data and micrographs suggest that, at the highest strains in this study, both strength and microstructure may be closest to reaching a steady state for foliations oriented 120–165°, which are in the P-orientation. This is consistent with the kinematic model of Cladouhos (1999) which suggests that the P-foliation is strain insensitive.

Earthquakes can be generated by foliation-parallel slip (Ferreira et al., 2008), however in many cases earthquakes induce motion that is accommodated by deformation away from the fault zone proper (Philip and Meghraoui, 1983; Klinger and Rockwell, 1987; Berberian et al., 1994; Lee et al., 2002). We observe that the velocity-dependence of friction for our intact, foliated rock samples appears to be lower, on average, than powder which is consistent with the idea that shear fabric development tends to reduce a - b and promote unstable frictional slip (Beeler et al., 1996; Marone, 1998). However, for our slate samples the a - b values are consistently positive, indicating an inability to nucleate earthquakes. Previous work with a wide range of rock types has shown that lithified, foliated rock is less likely to exhibit velocity-weakening than fabric-free, isotropic (or nearly isotropic) rocks such as granite and sandstone (Ikari et al., 2011). Therefore, it is likely that because deformation occurs on multiple localization features and is likely distributed across the rock fabric, the effect of rock foliation

on slip stability is minimal compared to other factors known to be important such as localization to a single, continuous plane (Logan et al., 1992; Scruggs and Tullis, 1998), mineralogic composition (Shimamoto and Logan, 1981; Ikari et al., 2011) and the operation of solution-transfer processes (Niemeijer and Spiers, 2006).

5. Conclusions

We show experimentally that pre-existing foliation in any orientation can lower the residual shear strength of rock, and that at very low shear strain the specific orientation can have a strong influence on failure strength and microstructural development. We present microstructural observations indicating that foliation-parallel slip, foliation-perpendicular fracturing, low-porosity compacted zones, active rotation, and wide through-going cataclastic zone formation are highly dependent on the pre-existing foliation orientation. We find that patterns in failure strength can generally be explained by considering whether the fabric is favorably or unfavorably oriented with respect to principal stress axes that have rotated to be 45° from the remotely applied stresses, rather than the shear direction itself. However, at higher strains through-going zones of deformation zones develop in the R1 orientation, which results in an apparent residual strength that is generally independent of the foliation orientation, but still lower than that of powdered slate. The development of these zones coincides with high measured rates of thinning and occur at higher strain when deformation is accommodated by large through-going cataclastic zones. We suggest that at high strains, the pre-existing foliation becomes less important, however the presence of any foliation still reduces the apparent fault strength.

Acknowledgments

We thank Peter Zavalij for XRD analysis, Sam Haines for XTG measurement, and Chris Spiers for helpful discussions. We also thank two anonymous reviewers for helpful comments that improved this manuscript. This work was partially supported by a European Research Council Starting Grant Project No. 205175 (USEMS, P.I. Giulio di Toro) and Dutch Foundation for Scientific Research (NWO) VENI grant no. 863.09.013, VIDI grant, no. 854.12.011, and ERC starting grant SEISMIC, no. 335915 to A. Niemeijer, by NSF grants OCE-0648331, EAR-0746192, and EAR-0950517 to C. Marone, and by an NRC-ISES Visiting Research Fellowship to M. Ikari.

References

- Attwell, P.B., Sandford, M.R., 1974. Intrinsic shear strength of a brittle, anisotropic rock – I. Experimental and mechanical interpretation. *Int. J. Rock Mech. Min. Sci. Geomech. Abstr.* 11, 423–430.
- Beeler, N.M., Tullis, T.E., Blanpied, M.L., Weeks, J.D., 1996. Frictional behavior of large displacement experimental faults. *J. Geophys. Res.* 101, 8697–8715.
- Becker, A., 1994. Bedding-plane slip over a pre-existing fault, an example: the Ramon Fault, Israel. *Tectonophysics* 230, 91–104.
- Bell, T.H., 1986. Foliation development and refraction in metamorphic rocks: reactivation of earlier foliations and deceleration due to shifting patterns of deformation partitioning. *J. Metamorph. Geol.* 4, 421–444.
- Berberian, M., Jackson, J.A., Qorashi, M., Talebian, M., Khatib, M., Priestley, K., 1994. The 1994 Sefidabeh earthquakes in eastern Iran: blind thrusting and bedding-plane slip on a growing anticline, and active tectonics of the Sistan suture zone. *Geophys. J. Int.* 142, 283–299.
- Bistacchi, A., Massironi, M., Menegon, L., Bolognesi, F., Donghi, V., 2012. On the nucleation of non-Andersonian faults along phyllosilicate-rich mylonite belts. In: Healy, D., Butler, R.W.H., Shipton, Z.K., Sibson, R.H. (Eds.), *Faulting, Fracturing and Igneous Intrusion in the Earth's Crust*, Geological Society of London, vol. 367, pp. 185–199. <http://dx.doi.org/10.1144/SP367.13>. Special Publications.
- Butler, R.W.H., Bond, C.E., Shipton, Z.K., Jones, R.R., Casey, M., 2008. Fabric anisotropy controls faulting in the continental crust. *J. Geol. Soc. London* 165, 449–452.
- Byerlee, J., 1978. Friction of rocks. *Pure Appl. Geophys.* 116, 615–626.

- Byerlee, J.D., Savage, J.C., 1992. Coulomb plasticity within the fault zone. *Geophys. Res. Lett.* 19 (23), 2341–2344.
- Carpenter, B.M., Marone, C., Saffer, D.M., 2011. Weakness of the San Andreas fault revealed samples from the active fault zone. *Nat. Geosci.* 4, 251–254. <http://dx.doi.org/10.1038/NGEO1089>.
- Chester, F.M., Friedman, M., Logan, J.M., 1985. Foliated cataclases. *Tectonophysics* 111, 139–146.
- Cladouhos, T.T., 1999. A kinematic model for deformation within brittle shear zones. *J. Struct. Geol.* 21, 437–448.
- Colletini, C., Sibson, R.H., 2001. Normal faults, normal friction? *Geology* 29 (10), 927–930.
- Colletini, C., Holdsworth, R.E., 2004. Fault zone weakening and character of slip along low-angle normal faults: insights from the Zuccale fault, Elba, Italy. *J. Geol. Soc. London* 16, 1039–1051.
- Colletini, C., Niemeijer, A., Viti, C., Marone, C., 2009. Fault zone fabric and fault weakness. *Nature* 462, 907–910. <http://dx.doi.org/10.1038/nature08585>.
- Craig, R.F., 2004. *Craig's Soil Mechanics*, seventh ed. Taylor & Francis, New York, NY.
- Davis, B.K., Forde, A., 1994. Regional slaty cleavage formation and fold axis rotation by re-use and reactivation of pre-existing foliations: the Fiery Creek Slate Belt, North Queensland. *Tectonophysics* 230, 161–179.
- Dieterich, J.H., 1979. Modeling of rock friction 1. Experimental results and constitutive equations. *J. Geophys. Res.* 84 (B5), 2161–2168.
- Dieterich, J.H., 1981. Constitutive properties of faults with simulated gouge. In: Carter, N.L., Friedman, M., Logan, J.M., Stearns, D.W. (Eds.), *Mechanical Behavior of Crustal Rocks*, Geophysical Monograph Series, vol. 24. AGU, Washington, D.C, pp. 102–120.
- Donath, F.A., 1961. Experimental study of shear failure in anisotropic rocks. *Geol. Soc. Am. Bull.* 72, 985–990.
- Fagereng, Å., Byrnes, G., 2015. A range of fault slip styles on progressively misoriented planes during flexural-slip folding, Cape Fold Belt, South Africa. *J. Struct. Geol.* 70, 158–169. <http://dx.doi.org/10.1016/j.jsg.2014.12.001>.
- Ferreira, J.M., Bezerra, F.H.R., Sousa, M.O.L., do Nascimento, A.F., Sá, J.M., Franca, G.S., 2008. The role of Precambrian mylonitic belts and present-day stress field in the coseismic reactivation of the Pernambuco lineament, Brazil. *Tectonophysics* 456, 111–126.
- Frost, E., Dolan, J., Ratschbacher, L., Hacker, B., Seward, G., 2011. Direct observation of fault zone structure at the brittle-ductile transition along the Salzach-Ennstal-Mariazell-Puchberg fault system, Austrian Alps. *J. Geophys. Res.* 116 <http://dx.doi.org/10.1029/2010JB007719>, B02411.
- Haines, S.H., van der Pluijm, B.A., Ikari, M.J., Saffer, D.M., Marone, C., 2009. Clay fabric intensity in natural and artificial fault gouges: implications for brittle fault zone processes and sedimentary basin clay fabric evolution. *J. Geophys. Res.* 114 <http://dx.doi.org/10.1029/2008JB005866>, B05406.
- Haines, S.H., Kaproth, B., Marone, C., Saffer, D., van der Pluijm, B., 2013. Shear zones in clay-rich fault gouge: a laboratory study of fabric development and evolution. *J. Struct. Geol.* 51, 206–225. <http://dx.doi.org/10.1016/j.jsg.2013.01.002>.
- Ham, A.P., Bell, T.H., 2004. Recycling of foliations during folding. *J. Struct. Geol.* 26, 1989–2009.
- Handin, J., 1969. On the Coulomb-Mohr failure criterion. *J. Geophys. Res.* 74 (22), 5343–5348.
- Hobbs, B.E., Ord, A., Marone, C., June, 1990. Dynamic behaviour of rock joints. In: Barton, N.R., Stephansson, O. (Eds.), *Proceedings of the International Symposium on Rock Joints*, pp. 435–445. Loen, Norway.
- Hoek, E., 1964. Fracture of anisotropic rock. *J. South Afr. Inst. Min. Metal.* 64 (10), 501–518.
- Hull, J., 1988. Thickness-displacement relationships for deformation zones. *J. Struct. Geol.* 10, 431–435.
- Ikari, M.J., Niemeijer, A.R., Marone, C., 2011. The role of fault zone fabric and lithification state on frictional strength, constitutive behavior, and deformation microstructure. *J. Geophys. Res.* 116 <http://dx.doi.org/10.1029/2011JB008264>, B08404.
- Jefferies, S.P., Holdsworth, R.E., Wibberley, C.A.J., Shimamoto, T., Spiers, C.J., Niemeijer, A.R., Lloyd, G.E., 2006. The nature and importance of phyllonite development in crustal-scale fault cores: an example from the Median Tectonic Line, Japan. *J. Struct. Geol.* 28, 220–235.
- Klinger, R.E., Rockwell, T.K., 1987. Flexural-slip folding along the eastern Elmore Ranch fault in the superstition hills earthquake sequence of November 1987. *Bull. Seismol. Soc. Am.* 79 (2), 297–303.
- Lee, J.-C., Chu, H.-T., Angelier, J., Chan, Y.-C., Hu, J.-C., Lu, C.-Y., Rau, R.-J., 2002. Geometry and structure of northern surface ruptures of the 1999 $M_w = 7.6$ Chi-Chi Taiwan earthquake: influence from inherited fold belt structures. *J. Struct. Geol.* 24, 173–192.
- Logan, J.M., Dengo, C.A., Higgs, N.G., Wang, Z.Z., 1992. Fabrics of experimental fault zones: their development and relationship to mechanical behavior. In: Evans, B., Wong, T.-F. (Eds.), *Fault Mechanics and Transport Properties of Rocks*. Academic Press, Ltd., San Diego, CA, pp. 33–67.
- Logan, J.M., 2007. The progression from damage to localization of displacement observed in laboratory testing of porous rocks. In: Lewis, H., Couples, G.D. (Eds.), *The Relationship between Damage and Localization*, vol. 289. Geological Society, London, pp. 75–87. Special Publications.
- Mandl, G., de Jong, L.N.J., Maltha, A., 1977. Shear zones in granular material. *Rock Mech.* 9, 95–144.
- Marone, C., 1991. A note on the stress-dilatancy relation for simulated fault gouge. *Pure Appl. Geophys.* 137, 409–419.
- Marone, C., 1995. Fault zone strength and failure criteria. *Geophys. Res. Lett.* 22, 723–726.
- Marone, C., 1998. Laboratory-derived friction laws and their application to seismic faulting. *Annu. Rev. Earth Planet. Sci.* 26, 643–696.
- Massironi, M., Bistacchi, A., Menegon, L., 2011. Misoriented faults in exhumed metamorphic complexes: rule or exception? *Earth Planet. Sci. Lett.* 307, 233–239. <http://dx.doi.org/10.1016/j.epsl.2011.04.041>.
- Niemeijer, A.R., Spiers, C.J., 2005. Influence of phyllosilicates on fault strength in the brittle-ductile transition: Insights from rock analogue experiments. In: Bruhn, D., Burlini, L. (Eds.), *High Strain Zones: Structure and Physical Properties*, vol. 245. Geological Society, London, pp. 303–327. Special Publications.
- Niemeijer, A.R., Spiers, C.J., 2006. Velocity dependence of strength and healing behavior in simulated phyllosilicate-bearing fault gouge. *Tectonophysics* 427, 231–253.
- Niemeijer, A.R., Marone, C., Elsworth, D., 2010. Fabric induced weakness of tectonic faults. *Geophys. Res. Lett.* 37 <http://dx.doi.org/10.1029/2009GL041689>, L03304.
- Philip, H., Meghraoui, M., 1983. Structural analysis and interpretation of the surface deformations of the El Asnam earthquake of October 10, 1980. *Tectonics* 2 (1), 17–49.
- Ramsay, J.G., 1974. Development of chevron folds. *Geol. Soc. Am. Bull.* 85, 1741–1754.
- Rathbun, A.P., Marone, C., 2010. Effect of strain localization on frictional behavior of sheared granular materials. *J. Geophys. Res.* 115 <http://dx.doi.org/10.1029/2009JB006466>, B01204.
- Ruina, A., 1983. Slip instability and state variable friction laws. *J. Geophys. Res.* 88 (B12), 10,359–10,370.
- Rutter, E.H., Maddock, R.H., Hall, S.H., White, S.H., 1986. Comparative microstructures of natural and experimentally produced clay-bearing fault gouges. *Pure Appl. Geophys.* 124, 3–30.
- Scholz, C.H., 1987. Wear and gouge formation in brittle faulting. *Geology* 15, 493–495.
- Scholz, C.H., 2002. *The Mechanics of Earthquakes and Faulting*, second ed. Cambridge Press, New York, NY.
- Scott, D.R., Marone, C.J., Sammis, C.G., 1994. The apparent friction of granular fault gouge in sheared layers. *J. Geophys. Res.* 99 (B4), 7231–7246.
- Scruggs, V.J., Tullis, T.E., 1998. Correlation between velocity dependence of friction and strain localization in large displacement experiments on feldspar, muscovite and biotite gouge. *Tectonophysics* 295, 15–40.
- Shimamoto, T., Logan, J.M., 1981. Effects of simulated clay gouges on the sliding behavior of Tennessee sandstone. *Tectonophysics* 75, 243–255.
- Sibson, R.H., 1985. A note on fault reactivation. *J. Struct. Geol.* 7 (6), 751–754.
- Sibson, R.H., 1986. Brecciation processes in fault zones: inferences from earthquake rupturing. *Pure Appl. Geophys.* 124, 159–175.
- Tanner, P.W.G., 1989. The flexural-slip mechanism. *J. Struct. Geol.* 11 (6), 635–655.
- Tesei, T., Colletini, C., Carpenter, B., Viti, C., Marone, C., 2012. Frictional strength and healing behaviour of phyllosilicate-rich faults. *J. Geophys. Res.* 117 <http://dx.doi.org/10.1029/2012JB009204>, B09402.